Research Square

Preprints are preliminary reports that have not undergone peer review.
They should not be considered conclusive, used to inform clinical practice,
or referenced by the media as validated information.

Single-cell transcriptomics reveals cellular heterogeneity of condylar chondrocytes in SD rat temporomandibular joint osteoarthritis

Feifei Xie
Yunnan Key Laboratory of Stomatology & Department of Orthodontics, The Affiliated Stomatology Hospital, Kunming Medical University

Yinzi Xin
Yunnan Key Laboratory of Stomatology & Department of Orthodontics, The Affiliated Stomatology Hospital, Kunming Medical University

Tao Xie
Yunnan Key Laboratory of Stomatology & Department of Orthodontics, The Affiliated Stomatology Hospital, Kunming Medical University

Jinghan Li
Yunnan Key Laboratory of Stomatology & Department of Orthodontics, The Affiliated Stomatology Hospital, Kunming Medical University

Jingpeng Zuo
Yunnan Key Laboratory of Stomatology & Department of Orthodontics, The Affiliated Stomatology Hospital, Kunming Medical University

Jiangtian Hu
Yunnan Key Laboratory of Stomatology & Department of Orthodontics, The Affiliated Stomatology Hospital, Kunming Medical University

Wei Wang
wangwei8@kmmu.edu.cn

Yunnan Key Laboratory of Stomatology & Department of Orthodontics, The Affiliated Stomatology Hospital, Kunming Medical University

Research Article

Keywords: Temporomandibular joint osteoarthritis, Single-cell RNA sequencing, Chondrocyte heterogeneity, S100a9, CAMP

Posted Date: November 17th, 2025

DOI: https://doi.org/10.21203/rs.3.rs-7638769/v1

License: This work is licensed under a Creative Commons Attribution 4.0 International License.
Read Full License

Additional Declarations: No competing interests reported.

Version of Record: A version of this preprint was published at BMC Oral Health on September 10th, 2026. See the published version at https://doi.org/10.1186/s12903-026-09753-x.

Abstract

Background

The differentiation of condylar chondrocytes plays a pivotal role in the pathogenesis of temporomandibular joint osteoarthritis (TMJOA). However, the characteristics of condylar chondrocyte subsets and their functional roles in TMJOA remain poorly defined. This study aims to investigate the heterogeneity and functional characteristics of condylar chondrocyte subsets in TMJOA.

Results

Micro-CT, histological and immunohistochemical staining confirmed successful establishment of the TMJOA model in CFA-induced SD rats. scRNA-seq identified 13 major cell types in the condylar cartilage and characterized three distinct chondrocyte subsets: homeostatic chondrocytes (HomCs), pre-inflammatory chondrocytes (preInfCs) and inflammatory chondrocytes (InfCs). Among them, InfCs exhibited high expression of S100a9 and CAMP, which were markedly upregulated at the terminal stage of InfC differentiation. Western blotting and qRT-PCR confirmed their elevated expression, while IHC and IF demonstrated strong co-localization of these markers in InfCs, predominantly located in the pre-hypertrophic and hypertrophic layers of the cartilage.

Conclusions

This study reveals the heterogeneity of chondrocytes in TMJOA and identifies three distinct subsets: HomCs, preInfCs and InfCs. $S100a9^{+}CAMP^{+}$ InfCs are primarily localized to the pre-hypertrophic and hypertrophic layers of condylar cartilage, where they are involved in signaling pathways related to cartilage matrix degradation. These findings enhance our understanding of the pathological mechanisms underlying TMJOA and provide a theoretical basis for the identification of potential therapeutic targets.

Background

Temporomandibular joint osteoarthritis (TMJOA) is a prevalent chronic degenerative joint disorder, with its incidence progressively increasing in parallel with global population aging[1,2]. Epidemiological studies have shown that the prevalence of TMJOA in the general population ranges from 8% to 16%, with a higher proportion observed in females, and it is often associated with other degenerative disorders[3,4]. The hallmark pathological features of TMJOA include degeneration of the articular cartilage, remodeling of the subchondral bone and inflammation of the synovial membrane[5,6]. Clinically, TMJOA is commonly manifested by facial pain, limited mandibular mobility, masticatory dysfunction and joint noises. With the progression of TMJOA, some individuals may experience marked limitations in mouth opening, along with impairments in speech and swallowing functions[7]. These

impairments significantly affect daily functioning and social interactions, ultimately leading to a reduced quality of life and increased healthcare burden. However, the complex pathophysiological mechanisms underlying TMJOA have hindered the development of effective diagnostic tools and therapeutic strategies. Therefore, in-depth investigation of inflammation-related pathological processes and the contributions of specific cellular populations to the onset and progression of TMJOA are essential for elucidating its underlying mechanisms and identifying potential therapeutic targets.

The mandibular condylar cartilage (MCC), a fibrocartilaginous structure with high elasticity, is essential for absorbing mechanical loads, reducing joint friction and preserving temporomandibular joint stability[8]. Anatomically, the MCC is organized into four distinct zones—superficial, proliferative, prehypertrophic and hypertrophic—each representing a specific stage of chondrocyte differentiation[9–11]. Under physiological conditions, chondrocytes within these zones exhibit unique morphological and functional characteristics that collectively maintain cartilage homeostasis and biomechanical integrity[12]. However, in inflammatory conditions such as TMJOA, chondrocyte phenotypes and functions become markedly disrupted[13]. Although substantial progress has been made in elucidating chondrocyte heterogeneity and functional dynamics in knee osteoarthritis, comprehensive studies of chondrocyte subsets within the MCC and their roles in TMJOA pathogenesis remain poorly understood.

The emergence of single-cell RNA sequencing (scRNA-seq) has enabled high-resolution characterization of gene expression profiles at the single-cell level. In osteoarthritis (OA) research, scRNA-seq offers unprecedented opportunities to dissect chondrocyte heterogeneity, uncover their interactions with other cell types and delineate the molecular pathways driving disease progression[14–16]. Several scRNA-seq studies have identified previously unrecognized chondrocyte subsets in knee OA, extending beyond the four conventionally defined types. These include effector chondrocytes (ECs), regulatory chondrocytes (RegCs), homeostatic chondrocytes (HomCs), pre-inflammatory chondrocytes (preInfCs) and inflammatory chondrocytes (InfCs)[17–19]. These newly identified subsets contribute to cartilage degeneration and heightened inflammation by activating the expression of inflammation-related genes and modulating cellular metabolic processes. However, research specifically addressing TMJOA remains limited. The cellular composition, disease-associated biomarkers and cellular heterogeneity underlying TMJOA pathogenesis remain poorly understood and require further investigation.

To bridge this knowledge gap, we constructed a complete Freund's adjuvant (CFA)-induced inflammatory TMJOA model in Sprague-Dawley (SD) rats and performed single-cell RNA sequencing to systematically map the cellular landscape of the mandibular condyle. We identified three transcriptionally and functionally distinct chondrocyte subsets. Among them, a previously uncharacterized subset, $S100a9^{+}$ (S100 calcium-binding protein a9) $CAMP^{+}$ (cathelicidin antimicrobial peptide) inflammatory chondrocytes appeared to be closely associated with TMJOA progression, potentially through dysregulation of mitochondrial metabolic pathways. We further validated the spatial distribution of this subset using immunohistochemistry and immunofluorescence (IF). Our study provides a comprehensive single-cell transcriptomic profile of MCC in the context of TMJOA, offering novel insights into

chondrocyte heterogeneity and regulatory mechanisms, and providing a foundation for the development of potential therapeutic targets.

Materials and methods

Establishment of a TMJOA model

A total of 12 six-week-old male SD rats (180–220g; purchased from the Experimental Animal Center of Kunming Medical University) were housed under controlled temperature conditions on a 12-hour light/dark cycle, with ad libitum access to food and water. The rats were randomly assigned to either the OA group or the negative control (NC) group (n = 6 per group). Anesthesia was administered via intraperitoneal injection of sodium pentobarbital (50 mg/kg body weight). To establish an inflammatory TMJOA rat model, we performed intra-articular injection of inflammatory reagent CFA (1:1 oil:saline emulsion; Sigma Aldrich, St. Louis, MO, USA) into the temporomandibular joints (TMJ) on Day 0 (primary injection) and Day 3 (secondary injection) to induce inflammation. Rats in the NC group received intra-articular injections of saline in the same volume. TMJ inflammation was assessed through physical examination and histological analysis. All experimental procedures were approved by the Animal Ethics Committee of Kunming Medical University (Approval No. KMMU20241904).

Tissue harvest

Ten days after CFA injection, the rats were euthanized by intraperitoneal injection of an overdose of sodium pentobarbital and positioned on the surgical table. The hair anterior to the auricular region was carefully removed. A scalpel was used to make an incision in the designated area, and the subcutaneous tissue was carefully dissected to avoid damaging the TMJ and surrounding structures. Using microsurgical instruments, the connection between the condyle and the joint capsule was carefully dissected to expose the condylar surface. The bilateral TMJ were excised from the mandibular ramus by transecting the condylar neck.

Micro-CT analysis

Collected TMJ tissues from each group were fixed in 4% paraformaldehyde solution for 24 h and flushed overnight. Afterwards, TMJ specimens used for bone morphological analysis were scanned by micro-CT (90 kV, 100 μA·s, 4.6 μm/pixel resolution) to assess changes in the subchondral bone. The acquired data were reconstructed using Avatar software to obtain three-dimensional images for morphological assessment. Subsequently, sagittal sections were generated for quantitative evaluation. The largest sagittal section of the condyle was selected, and three cubic regions of interest (0.3 mm × 0.3 mm × 0.3 mm) were defined at the anterior, middle and posterior regions near the bone–cartilage interface. The following parameters were measured and analyzed: bone volume fraction (BV/TV), trabecular thickness (Tb.Th), trabecular number (Tb.N) and trabecular separation (Tb.Sp).

Histology for TMJOA and scoring

The harvested condylar tissues were fixed in 4% paraformaldehyde for 24 hours. The samples were subsequently decalcified in EDTA solution for 7 days. Following dehydration and paraffin embedding, serial sagittal sections of the condylar tissue were prepared at a thickness of 4 μm. Histological sagittal sections of the TMJs were subjected to Hematoxylin and Eosin (HE) and Safranin O–Fast Green staining to assess histological changes in the joints. Condylar cartilage destruction was evaluated using the Osteoarthritis Research Society International (OARSI) scoring system and the modified Mankin scoring system by three independent observers blinded to the experimental conditions. The OARSI scores ranged in each case from 0 to 6 points, where 0 indicated no evidence of OA and higher scores indicated a more severe OA phenotype, characterized by unclear borders between cartilage and subchondral bone, uneven cartilage surfaces and decreased hypertrophic layer thickness[20]. The modified Mankin scoring system evaluated four parameters: cartilage surface damage (0–2), loss of cellularity (0–2), reduction in matrix staining (0–2), and disruption of tidemark integrity (0–2). Higher scores reflect increased severity of TMJOA[21].

Immunohistochemistry

Sections for immunohistochemical analysis were first dewaxed in xylene and then rehydrated through a graded ethanol series. Antigen retrieval was performed using 0.01 M citrate buffer at 95°C, followed by cooling to room temperature. Sections were incubated with 3% hydrogen peroxide for 5 minutes to inactivate endogenous peroxidase, followed by overnight incubation at 4°C with primary antibodies against matrix metalloprotein13 (MMP13) (ab39012, Abcam, Cambridge, UK), interleukin-1β (IL-1β) (ab283818, Abcam, Cambridge, UK), Aggrecan (ab313636, Abcam, Cambridge, UK) and collagen type II (COL2) (ab34712, Abcam, Cambridge, UK). Sections were then rinsed with PBS, incubated with HRP-conjugated secondary antibodies for 15 minutes and developed with DAB for 5 minutes. Immunoreactivity was visualized using a Zeiss microscope (Carl Zeiss MicroImaging, Oberkochen, Germany) and quantified with ImageJ software (NIH, Bethesda, MD, USA).

Immunofluorescence

Sections were dewaxed in xylene and rehydrated through a graded ethanol series. Antigen retrieval was performed in 0.01 M sodium citrate buffer (pH 6.0) at 95°C for 30 minutes, followed by cooling to room temperature and three washes with PBS. Subsequently, sections were incubated with 0.3% Triton X-100 (T8787, Sigma-Aldrich, St. Louis, MO, USA) at room temperature for 15 minutes to enhance membrane permeability, followed by washing with PBS. Non-specific binding was blocked with 5% bovine serum albumin (BSA) for 1 hour at room temperature. After blocking, sections were incubated overnight at 4°C with primary antibodies against S100a9 (ab242945, Abcam, Cambridge, UK) and CAMP (ab76238, Abcam, Cambridge, UK). The following day, after washing with PBS, sections were incubated in the dark at 37°C for 1 hour with Alexa Fluor 488-conjugated anti-rabbit secondary antibody (A-11008, Thermo

Fisher Scientific, Waltham, MA, USA) (for S100a9) and Alexa Fluor 594-conjugated anti-rabbit secondary antibody (A-11012, Thermo Fisher Scientific, Waltham, MA, USA) (for CAMP). Nuclei were counterstained with DAPI (D9542, Sigma-Aldrich, St. Louis, MO, USA) for 5 minutes, followed by washing with PBS. Finally, an anti-fade mounting medium (Fluoromount-G®, 0100-01, SouthernBiotech, Birmingham, AL, USA) was applied dropwise, and fluorescence imaging was performed using a fluorescence microscope (Carl Zeiss, Oberkochen, Germany). The number of positively stained cells was quantified using ImageJ (NIH, Bethesda, MD, USA) for subsequent analysis.

Single-cell RNA sequencing

This study utilized 10x Genomics scRNA-seq technology to perform transcriptomic analysis of condylar chondrocytes in SD rats, aiming to decipher the cellular heterogeneity in TMJOA. Condylar cartilage tissues were enzymatically digested using a dissociation solution containing 0.35% collagenase IV (C5138, Sigma-Aldrich, St. Louis, MO, USA), 2.5 mg/mL papain (P4762, Sigma-Aldrich, St. Louis, MO, USA) and 120 U/mL DNase I (10104159001, Roche, Basel, Switzerland) to prepare a single-cell suspension, which was subsequently processed using the Chromium Single Cell 3' Reagent Kit v3.1 (10x Genomics, Pleasanton, CA, USA) on the Chromium platform for single-cell capture. Through microfluidic technology, single cells were encapsulated with gel beads containing unique barcodes (GEMs) using the Chromium Single Cell 3' Reagent Kit v3.1 (10x Genomics, Pleasanton, CA, USA) to form individual reaction units. Reverse transcription and library construction were performed according to the manufacturer’s protocol. High-throughput sequencing was conducted on the NovaSeq 6000 platform (Illumina, San Diego, CA, USA) to ensure single-cell resolution and data quality. The sequencing data were aligned to the rat reference genome (Ensembl release 110) using Cell Ranger software (v7.2.0, 10x Genomics, Pleasanton, CA, USA) and a gene expression matrix was generated for downstream analysis.

Quality control, dimension-reduction and clustering

All analyses were performed in R (v4.2.2, R Foundation for Statistical Computing, Vienna, Austria). The Seurat package (v 5.0.1, developed by Satija Lab, New York Genome Center, USA) was utilized to perform quality control (QC) and downstream analysis of the scRNA-seq data[22]. To ensure the reliability of the data, initial filtering was conducted to remove cells expressing fewer than 200 genes and genes detected in fewer than 3 cells. The QC was performed according to the following specific criteria: 1) deleting genes that were expressed in less than 3 cells, 2) deleting cells with gene numbers lower than 200 or higher than 6000, 3) deleting cells with the sum of gene expression numbers lower than 500 or higher than 10,000, and 4) deleting cells with the proportion of mitochondrial genes greater than 10%. After filtering out the cells and genes that did not meet the criteria, NormalizeData function was employed to normalize the data (normalization.method = “LogNormalize” and scale.factor = 10000). Then the FindVariableFeatures function was used to extract the top 2000 highly variable genes (HVGs), and the result was shown by LabelPoints (the 10 HVGs with the largest variation were labeled). Furthermore,

HVGs were subjected to principal components analysis (PCA). The appropriate principal components (PCs) were selected using the JackStraw and Elbowplot functions.

Next, the resolution was set to 0.4, the cells were subjected to unsupervised cluster analysis using the rs FindNeighboand FindClusters functions of the Seurat package (v 5.0.1). The results of clustering were visualized using the uniform manifold approximation and projection (UMAP) algorithm.

Cell type recognition and cellular communication

Subsequently, the marker genes were applied to annotate cell types of the different clusters. The annotation results were visualized in a UMAP plot. The proportions of different cell types in TMJOA samples and control samples were further visualized. Key cells were obtained based on other literature. Moreover, cell-type interactions were probed using CellChat package (v 1.6.1, developed by Jin Lab, Harvard Medical School, Boston, MA, USA), followed by visualization of cell-cell ligand-receptor pair interactions[23].

Functional enrichment analysis of key cell subsets

All samples in scRNA-seq data were enriched using the ReactomeGSA package (v1.16.1, developed by the European Bioinformatics Institute, Hinxton, UK) to explore the functions and pathways in which key cell subtypes were involved[24]. Afterward, differential analysis of each of the key cellular subtypes in the control and TMJOA groups was performed using the FindMarkers function (|log2fold change (FC) |>0.25, adj. $P < 0.05$, pt.1 > 0.1, pt.2 > 0.1), and the differential genes were subjected to Gene Ontology (GO), which involved biological processes (BP), cellular components (CC), and molecular functions (MF), and Kyoto Encyclopedia of Genes and Genomes (KEGG) enrichment analyses ($P < 0.05$).

Cellular communication and pseudo-time analyses of key cell subsets

First, the proportions of key cell subtypes were analyzed for differences using t-test ($P < 0.05$). Next, cell communication was analyzed for key cell subtypes using the CellChat package (v1.6.1, developed by Jin Lab, Harvard Medical School, Boston, MA, USA). Besides, each key cell subtype was re-descended and clustered. Pseudo-time analysis was performed using the Monocle package (v2.26.0, developed by Cole Trapnell Lab, University of Washington, Seattle, WA, USA).

Reverse transcription quantitative polymerase chain reaction

Approximately 20 mg of condylar surface cartilage tissue was thoroughly ground in liquid nitrogen using a mortar and pestle, and total RNA was extracted using Trizol reagent (R0016, Beyotime, Shanghai, China) according to the manufacturer's instructions. RNA yield was determined by measuring absorbance at 260 nm, and purity was assessed by the A260/A280 ratio using a NanoPhotometer NP80 (Implen GmbH, Munich, Germany). One microgram of total RNA was reverse transcribed into cDNA using

the RT First Strand cDNA Synthesis Kit (G3330, Servicebio, Wuhan, China). Real-time quantitative PCR (qRT-PCR) was performed on an MX3005P Real-Time PCR System (Agilent Technologies, Santa Clara, CA, USA) using SYBR Green qPCR Master Mix (RR420A, Takara, Shiga, Japan). GAPDH was used as the internal reference gene, and relative gene expression levels were calculated using the 2^−ΔΔCT method. The sequence-specific primers used for cDNA amplification are listed in Table 1.

Table 1
PCR primer sequences for target genes

GENE	Primer sequence forward	Primer sequence reverse
S100a9	TGGCTGCCAAAACAGGATCT	AATTCCGCCTTGTTCAGGGT
CAMP	CAGGGGGTAGTGAAGCAGTG	GCTGTATACCAGGCGCATCA
IL-1β	GTGCTGTCTGACCCATGTGA	GATTCTTCCCCTTGAGGCCC
MMP13	TTCTGGTCTTCTGGCACACG	TGGCTTTTGCCAGTGTAGGT
ADAMTS5	CCCAAATACGCAGGTGTCCT	ACACACGGAGTTGCTGTAGG
COL2A1	CACCGCTAACGTCCAGATGA	GTTTCGTGCAGCCATCCTTC
GAPDH	AGAGACAGCCGCATCTTCTT	TTCTCAGCCTTGACTGTGCC

Western Blot

Condylar cartilage samples were placed on ice, and total protein was extracted using RIPA lysis buffer (P0013B, Beyotime, Shanghai, China). Tissue lysates were homogenized and centrifuged at 10,000 × g for 10 minutes to collect the supernatant. Protein concentrations were determined using the Q3000 protein analyzer (Q3000, Semmerfeld, Shanghai, China). Western blot (WB) experiments were performed according to the manufacturer's instructions for the PAGE gel kit (P1200, Solebold, Beijing, China) and PVDF membranes. Membranes were incubated with the primary antibody overnight at 4°C, followed by incubation with the secondary antibody at room temperature for 1 hour. Protein band intensity was quantified using Quantity One software (Bio-Rad, Hercules, CA, USA). Western blotting was performed using primary antibodies against S100a9 (ab242945, Abcam, Cambridge, UK), CAMP (ab76238, Abcam, Cambridge, UK), MMP13 (ab39012, Abcam, Cambridge, UK), IL-1β (ab283818, Abcam, Cambridge, UK), a disintegrin and metalloproteinase with thrombospondin motifs 5 (ADAMTS5) (ab231595, Abcam, Cambridge, UK) and GAPDH (ab181602, Abcam, Cambridge, UK), along with an HRP-conjugated secondary antibody (ab205718, Abcam, Cambridge, UK).

Statistical Analysis

The R language (v4.2.2, R Foundation for Statistical Computing, Vienna, Austria) was used to conduct bioinformatics analyses. GraphPad Prism 10 (GraphPad Software, Inc., La Jolla, CA, USA) was used for the statistical analysis. All experimental data are expressed as means ± SD. Besides, the t-test was

employed in this study to assess differences between groups, setting the significance threshold at $P < 0.05$.

Results

Establishment of the Inflammatory Model of TMJ

To establish an inflammatory TMJOA rat model, we performed intra-articular injection of inflammatory reagent CFA into both sides of the TMJ to induce inflammation. Intense swelling and redness over the TMJ region were observed 10 days after the first CFA injection, but not in the NC group. The linear head width of the bilateral TMJs showed marked increases in the OA group (Fig. 1A). To examine whether CFA could induce degenerative processes in the SD rat model, micro-CT imaging was used to analyze bone architecture. There was a substantial morphological change in the subchondral bone in OA group compared with the NC group (Fig. 1, B and C). CFA-treated TMJ exhibited a substantial reduction in BV/TV, Tb.Th and Tb.N ($P < 0.05$, Fig. 1, D, E and F), as well as a robust increase in Tb.Sp ($P < 0.05$, Fig. 1G).

To further examine the pathologies, we performed HE staining of the TMJ at 10 days after CFA intra-articular injection. HE staining revealed several characteristic alterations in the condylar cartilage of the OA group compared with the NC group (Fig. 1H). The cartilage thickness was significantly reduced, and the chondrocyte layer organization was disrupted. In some areas, the arrangement of chondrocytes was disordered or even absent, manifesting as sparse chondrocytes and faint staining of the extracellular matrix, indicating cartilage degeneration. In contrast, in certain pathological regions, chondrocytes were clustered, suggesting chondrocyte proliferation or reactive changes. Additionally, the subchondral bone exhibited uneven bone density, with some areas showing thinning of trabeculae and widening of gaps, which may be associated with bone structural remodeling related to OA. Meanwhile, the OA group exhibited higher OARSI scores compared to the NC group ($P < 0.0001$, Fig. 1J). Safranin O-Fast Green staining revealed significant inflammatory changes in the condylar cartilage of the OA group compared to the NC group (Fig. 1I). Safranin O–Fast Green staining revealed pronounced inflammatory changes in the condylar cartilage of the OA group compared to the NC group, including decreased cartilage matrix content and increased proliferation of collagen fibers. Consistently, the modified Mankin scores were significantly elevated in CFA-injected rats, whereas saline-injected control displayed markedly lower scores ($P < 0.001$, Fig. 1K). In addition, immunohistochemical (IHC) revealed elevated expression of the classical inflammatory markers MMP13 and IL-1β in the OA group, whereas the expression of Aggrecan and COL2 was markedly reduced ($P < 0.05$, Fig. 1, L and M). Collectively, these results confirm that intra-articular injection of CFA effectively induces TMJOA in this experimental model.

The single-cell landscape of SD Rat Condylar Tissues

To comprehensively characterize the cellular landscape of condylar tissue in the TMJ, we performed scRNA-seq on a total of eight condylar samples, including five from the OA and three from the NC group (Fig. 2A). After implementing quality control exclusion, 53,428 single cells were retained, with the gene

count remaining unchanged at 20,471 (Fig. S1A and B). The top 2000 HVGs and 30 PCs were selected for cell clustering (Fig. S1C, D, E and F). The UMAP clustering classified the cells into 24 cell clusters (resolution = 0.4, Fig. 2B), which were annotated by marker genes into 13 cells types, namely B cells, chondrocytes, neutrophils, fibroblasts, monocytes, macrophages, osteoblasts, erythrocytes, T cells, brain microvascular endothelial cells (BMECs), basophils, pericytes and other cells (Fig. 2C). The bubble chart showed the marker gene expression levels associated with each cell population (Fig. 2E). The distribution of cell types differed between TMJOA and control groups (Fig. 2D). Subsequently, we assessed the fold-change differences across cell populations between the OA and NC groups and performed a comparative analysis of cell type proportions (Fig. 2F). Notably, monocytes, macrophages, erythrocytes, and T cells were enriched in the OA group relative to the NC group ($P < 0.05$, Fig. 2G).

To investigate intercellular communication and infer the interactions between different cell types, we conducted an intercellular communication analysis across 13 cell types, with the results presented in a cell interaction network diagram (Fig. S2A, B, C and D). The analysis revealed that fibroblasts and osteoblasts exhibited close communication in both groups. Additionally, erythrocyte communication was observed in the OA group, a phenomenon absent in the NC group. Further analysis demonstrated that intercellular communication was more prominent in the OA group compared to the NC group, with a significant increase in both the strength and frequency of communication between chondrocytes and fibroblasts as well as macrophages.

The cell-cell communication heatmap revealed that, in the NC group, intercellular interactions were relatively sparse and limited to a few specific cell types. Notable signaling was primarily observed between fibroblasts and immune cells such as macrophages and monocytes, while chondrocytes exhibited minimal interaction with other populations. In contrast, the OA group showed a marked increase in the overall number of intercellular interactions, with more extensive and tightly connected signaling networks among diverse cell types. Interactions involving fibroblasts, macrophages, monocytes and BMECs were particularly intensified. Furthermore, inflammatory cells, including macrophages, monocytes and T cells, demonstrated enhanced communication with chondrocytes and osteoblasts (Fig. 2H and I). These findings suggest that the OA microenvironment is characterized by significantly elevated intercellular communication, especially involving immune-related cell populations.

Heterogeneity analysis of TMJ chondrocyte subsets

We subsequently focused on the chondrocyte population, which was further subdivided into three distinct subtypes: Chondrocyte 1 (Bglap, LOC120102105, ENSRNOG00000063301 and AABR07060872.1), Chondrocyte 2 (Col5a1, Aebp1, Col15a1 and Prelp) and Chondrocyte 3 (S100a9, CAMP, Lcn2 and Ngp, Fig. 3A and B). A corresponding bar chart revealed that Chondrocyte 1 was more prevalent in the NC group, whereas Chondrocyte 3 was enriched in the OA group (Fig. 3C). To explore the specific biological functions of each subset, we next investigated the functional pathways of each chondrocyte subset.

GO enrichment analysis revealed that the differentially expressed genes (DEGs) associated with Chondrocyte 1 were predominantly enriched for terms related to protein folding, cellular respiration, ribosomes, mitochondrial protein complexes and ribosomal structural components (Fig. S3A). KEGG pathway analysis showed significant enrichment in pathways including Parkinson's disease, prion disease, amyotrophic lateral sclerosis, oxidative phosphorylation, and Huntington's disease-highlighting a strong association with mitochondrial function (Fig. S3B).

GO enrichment analysis showed that the DEGs in Chondrocyte 2 were mainly associated with key biological processes such as mRNA processing, RNA splicing, ribonucleoprotein complex biogenesis, proteasome-mediated ubiquitin-dependent protein catabolic process, and the establishment of protein localization to organelles-reflecting active involvement in gene regulation, protein synthesis, trafficking, and degradation (Fig. S3C). KEGG pathway analysis revealed significant enrichment in pathways related to neurodegenerative diseases, including Parkinson's disease, Huntington's disease, prion disease, protein processing in the endoplasmic reticulum, and amyotrophic lateral sclerosis. These findings suggest that Chondrocyte 2 may contribute to TMJOA pathogenesis through mechanisms involving impaired proteostasis and cellular stress responses (Fig. S3D).

GO enrichment analysis revealed that the DEGs in Chondrocyte 3 were significantly associated with key biological processes such as RNA splicing, mRNA processing, protein folding, proteasome complex formation, mitochondrial protein complex assembly, and translational regulation (Fig. S3E). These pathways are central to gene expression control, protein processing, and degradation. KEGG pathway analysis highlighted enrichment in several neurodegeneration-related pathways, including Parkinson's disease, Huntington's disease, prion disease, Alzheimer's disease, and amyotrophic lateral sclerosis. These pathways are closely linked to impaired protein homeostasis and cellular stress responses (Fig. S3F). Collectively, these findings suggest that Chondrocyte 3 may play a role in TMJOA by contributing to protein quality control and cellular homeostasis.

Chondrocyte 3 displayed enhanced enrichment in distinct pathways in both the OA and NC groups, notably including "glycerol transport from adipocytes to the liver via aquaporins," "synthesis of hepoxilins (HX) and trioxilins (TrX)" and the "fatty acid cycling model" (Fig. 3D). GO and KEGG enrichment analyses of DEGs across Chondrocyte subsets 1, 2 and 3 revealed significant overlap in pathways associated with mitochondrial function, such as "mitochondrial protein-containing complex" (GO:0098798), as well as neurodegeneration-related KEGG pathways including "Parkinson's disease," "Prion disease" and "Huntington's disease." These findings suggest that mitochondrial dysfunction and dysregulated neurodegenerative signaling may contribute to the pathogenesis of TMJOA, potentially affecting chondrocyte metabolism and stress responses. The involvement of these pathways indicates a possible mechanistic convergence between TMJOA and neurodegenerative disorders.

Dissecting the interactions among condylar chondrocyte subsets will help elucidate the mechanisms by which chondrocytes contribute to the pathogenesis of TMJOA. Intercellular communication analysis was performed among the three chondrocyte subsets. Compared to the NC group, the OA group showed a

decrease in both the number and strength of interactions between Chondrocyte 3 and Chondrocyte 2, while interactions between Chondrocyte 2 and Chondrocyte 1 were markedly increased (Fig. 3E and F). In the NC group, communication was relatively sparse, predominantly occurring between Chondrocyte 2 and Chondrocyte 3, with Chondrocyte 1 exhibiting limited interactions. In contrast, the OA group exhibited enhanced overall intercellular communication, particularly between Chondrocyte 2 and Chondrocyte 3 and Chondrocyte 1 also became more actively involved (Fig. S2E, F, G and H).

Bubble plots illustrated the predicted ligand–receptor interactions among all identified cell subsets. In the NC group, the predominant signaling event among chondrocyte subsets involved the interaction between Pleiotrophin (Ptn) and its receptor Syndecan-4 (Sdc4), with Chondrocyte 3 acting as the sender and Chondrocyte 2 as the receiver (Fig. S3G). A similar communication pattern was observed in the OA group, where Ptn released by Chondrocyte 3 continued to signal through Sdc4 on Chondrocyte 2 (Fig. S3H). Notably, an additional ligand–receptor pair emerged in the OA group: Chondrocyte 1 secreted Secreted Phosphoprotein 1 (SPP1), which interacted with Integrin receptors Itgav and Itgb1 expressed on Chondrocyte 2. This finding highlights an OA-specific enhancement of intercellular signaling between chondrocyte subsets.

Next, to investigate the lineage trajectories of condylar chondrocyte subsets, we performed pseudotime analysis to depict the dynamic changes in cellular composition during the progression from the healthy state to TMJOA. In the pseudotime analysis of chondrocyte subsets, chondrocytes differentiated from right to left along the trajectory (Fig. 3G), passing through five distinct differentiation states (Fig. S3H). Chondrocyte 2 was positioned at the early phase of the trajectory, suggesting it may represent an initial state of chondrocytes. Chondrocyte 1 occupied an intermediate position, indicating a transitional phase. In contrast, Chondrocyte 3 was primarily located at the terminal end of the trajectory (Fig. 3I), suggesting it may represent a more mature or functionally specialized chondrocyte state, which aligns with the observed increase in Chondrocyte 3 in the OA group.

Our analysis revealed that Chondrocyte 3 was positioned at the terminal end of the pseudotime trajectory, with a significantly increased proportion in the TMJOA group. These cells expressed Ptn, a factor associated with inflammation and tissue remodeling. Based on these findings, we classified Chondrocyte 3 as InfCs. In contrast, Chondrocyte 2 was located at the early stage of the pseudotime trajectory, suggesting that it represents an early inflammatory response phenotype. Under inflammatory conditions, the communication strength of Chondrocyte 2 gradually declined, indicating a potential loss of homeostatic regulatory function and a transition toward the Chondrocyte 3 phenotype. We therefore designated this subset as preInfCs. Conversely, Chondrocyte 1 was predominantly located at the intermediate stage of the pseudotime trajectory, potentially representing homeostatic or healthy chondrocytes. In the OA group, the proportion of Chondrocyte 1 was reduced, indicating that inflammation disrupted the maintenance of chondrocyte homeostasis. Moreover, Chondrocyte 1 was associated with SPP1, suggesting its involvement in chondrocyt-subchondral bone interactions and its potential role in repair. Accordingly, we defined this subset as HomCs.

Re-clustering and pseudotime analysis of HomCs, preInfCs and InfCs

To gain a more refined understanding of cellular heterogeneity and delineate distinct functional states, we performed reclustering of the chondrocyte subsets. Based on the expression of key marker genes, HomCs were further subdivided into three distinct subsets. HomCs-1 (red) and HomCs-2 (green) occupied two major regions of the UMAP space, while HomCs-3 (blue) formed a small, separate cluster, indicating a unique transcriptional identity (Fig. 4A). Bubble plot analysis highlighted marked differences in gene expression among the subsets—for example, Cd74 and Lyz2 were enriched in HomCs-2, while Comp and Cdkn1c were predominantly expressed in HomCs-1 (Fig. 4B). HomCs-3 exhibited a distinct transcriptional profile, further supporting its classification as a functionally specialized subset. Pseudotime analysis revealed that HomCs undergo a continuum of transitional states during differentiation (Fig. S4A). The annotated branch points (nodes 1 and 2) likely represent critical stages or transitional checkpoints along the differentiation trajectory. The HomC subsets progressed from right to left along the pseudotime axis and were classified into five distinct differentiation states (Fig. S4B), with HomCs-3 positioned at the terminal end of the trajectory (Fig. 4C), suggesting a more differentiated or specialized phenotype.

Next, preInfCs were further classified into four distinct subclusters based on key gene expression profiles. Among them, preInfCs-1 (red) and preInfCs-2 (green) were primarily distributed in two major regions of the UMAP space, whereas preInfCs-3 (blue) and preInfCs-4 (purple) were less abundant and localized to two smaller regions (Fig. 4D). Bubble plot analysis demonstrated marked differences in gene expression among these subsets (Fig. 4E). For instance, Col10a1 and Myl3 were highly expressed in preInfCs-1, while F13a1 and Defa5 were more prominent in preInfCs-2. Tmem255b and Clip2 exhibited specific expression patterns in preInfCs-3, and Ramp1 and Enho showed distinct expression in preInfCs-4. These transcriptional differences highlight the functional and phenotypic heterogeneity within the preInfCs subsets. Pseudotime analysis demonstrated a continuous progression of cellular states within the preInfCs subsets. Three key branching points (nodes 1, 2, and 3) likely represent critical transitions during differentiation (Fig. S4C). The trajectory revealed seven distinct differentiation states, with preInfCs-1 and preInfCs-2 predominantly located at the early stages, while preInfCs-3 and preInfCs-4 occupied terminal positions, suggesting a more advanced or specialized cell state (Fig. S4D).

Finally, to examine the expression changes of biomarkers during the transition of InfCs, we classified the InfCs subsets based on the expression of S100a9 and CAMP. The re-clustered and dimensionally reduced InfCs were categorized into two distinct subgroups: $S100a9^{+}CAMP^{+}$ InfCs and $S100a9^{-}CAMP^{-}$ InfCs, with the majority falling into the $S100a9^{+}CAMP^{+}$ InfCs group (Fig. 4G). The bubble plot demonstrates the gene expression profiles of the different InfCs subsets, revealing that S100a9 and CAMP show notably higher average expression levels in the $S100a9^{+}CAMP^{+}$ InfCs group (Fig. 4H). Pseudotime analysis revealed that InfCs differentiated from right to left over time, undergoing a continuous series of state transitions. The annotated key nodes (1, 2, 3, 4) likely represent critical

differentiation stages or transition points (Fig. S4E). Nine distinct differentiation states were observed within the InfCs (Fig. S4F). The S100a9^{+}CAMP^{+} InfCs are located at the end of the pseudotime trajectory, potentially representing chondrocytes in a highly inflammatory state, while the S100a9^{-}CAMP^{-} InfCs appear at earlier differentiation stages or in cell populations with lower inflammatory levels (Fig. 4I).

Characterisation of InfCs

We identified that gene expression in the InfCs subset was predominantly enriched in inflammation-related processes, including fatty acid cycling and the biosynthesis of HX and TrX. The proportion of InfCs was markedly increased in the OA group. Notably, S100a9^{+}CAMP^{+} InfCs represented the dominant subset and were positioned at the terminal stage of the inflammatory trajectory. To validate the expression of the InfC marker genes identified by scRNA-seq, we assessed S100a9 and CAMP expression in condylar cartilage tissues. WB analysis showed significantly elevated protein levels of the inflammatory markers ADAMTS5, IL-1β, and MMP13 in the OA group compared to the NC group, along with marked upregulation of S100a9 and CAMP ($P < 0.01$, Fig. 5A and B). These findings were further supported by qRT-PCR, which revealed increased mRNA expression of ADAMTS5, IL-1β, and MMP13 in the OA group, whereas expression of the cartilage matrix gene COL2A1 was significantly reduced. S100a9 and CAMP transcripts were also significantly upregulated, consistent with the protein-level results ($P < 0.05$, Fig. 5C).

To validate the presence and spatial distribution of InfCs in cartilage tissue, we conducted IHC staining for S100a9 and CAMP in condylar cartilage from OA and NC rats. A marked increase in the expression of both markers was observed in chondrocytes from the OA group compared to the NC group ($P < 0.001$, Fig. 5D and F). Notably, S100a9 and CAMP were primarily localized to the pre-hypertrophic and hypertrophic layers of the cartilage, suggesting that InfCs were mainly distributed within these specific zones of the cartilage structure.

Further IF co-staining assay demonstrated that S100a9 and CAMP were primarily localized in the pre-hypertrophic and hypertrophic zones of condylar cartilage in the OA group, consistent with the spatial distribution observed in the IHC analysis (Fig. 5E). A closer examination of these zones revealed markedly increased fluorescence intensity and broader distribution of both markers in OA cartilage compared to the NC group ($P < 0.01$, Fig. 5G). Notably, S100a9 and CAMP exhibited strong co-expression, further supporting the presence of a distinct inflammatory chondrocyte population within these cartilage layers.

Discussion

Chondrocyte heterogeneity is increasingly recognized as a key contributor to the onset and progression of osteoarthritis[14,19]. However, the cellular composition and functional diversity of chondrocytes in TMJOA remain poorly defined. In this study, we employed single-cell transcriptomic profiling to construct a comprehensive cellular atlas of the condylar cartilage and identified three transcriptionally distinct chondrocyte subsets: HomCs, preInfCs and InfCs. Among these, the InfC subset, characterized by

elevated expression of S100a9 and CAMP, was predominantly enriched in the OA group and localized to the pre-hypertrophic and hypertrophic zones of the cartilage. This spatial distribution and transcriptional profile suggest that InfCs are actively involved in inflammation-driven cartilage degradation. Our findings highlight the functional specialization of chondrocyte subsets in TMJOA and uncover previously unrecognized molecular features, which may contribute to understanding disease pathogenesis.

Our study identified 13 distinct cell types within the TMJ condyle of SD rats. In the OA group, the proportions of immune cells including monocytes, macrophages, erythrocytes and T cells increased, whereas the proportion of chondrocytes decreased. This shift may reflect immune cell involvement in chondrocyte damage or apoptosis triggered by inflammatory conditions. Macrophages play a pivotal role in the progression of OA by secreting pro-inflammatory cytokines such as IL-1β and tumor necrosis factor-α (TNF-α), which disrupt chondrocyte metabolic homeostasis, leading to cartilage matrix degradation and cellular damage. Similarly, Li et al. reported that during OA-associated inflammation, classically activated macrophages (M1 macrophages) become activated and secrete high levels of pro-inflammatory cytokines such as IL-1β, IL-6 and TNF-α. These cytokines stimulate the expression of MMPs, thereby accelerating cartilage degradation[25]. These studies suggest that immune cells, particularly macrophages, contribute to OA progression by promoting chondrocyte damage and cartilage degradation. Cell-cell communication analysis revealed markedly enhanced interactions among fibroblasts, macrophages and chondrocytes under inflammatory conditions. Consistent with this, Xie et al. reported that in knee OA, M1 macrophages enhance MMP secretion through interactions with synovial fibroblasts and chondrocytes, thereby contributing to subchondral bone remodeling, sustaining the inflammatory microenvironment and promoting disease progression[26]. Our findings support the notion that chondrocytes interact with multiple cell types, thereby contributing to the progression of TMJOA.

Accumulating evidence indicates that chondrocyte heterogeneity plays a critical role in the onset and progression of OA[27]. Sebastian et al. identified nine chondrocyte subsets with distinct molecular signatures in a murine model of traumatic OA[28]. Several of these subsets were enriched in inflammatory and catabolic pathways, underscoring their regulatory roles in inflammation and highlighting dynamic transcriptional changes during the early stages of OA. Ji et al. identified seven distinct chondrocyte subsets in human knee osteoarthritic cartilage and proposed a potential transition among proliferative, prehypertrophic and hypertrophic states, suggesting lineage plasticity under inflammatory conditions[29]. Recently, Fan et al. identified nine previously characterized chondrocyte subsets and two novel populations in human knee OA cartilage: preInfCs and InfCs. Both populations exhibited elevated inflammatory scores, and their upregulated genes were strongly associated with OA progression[17].

TMJOA exhibits a distinct chondrocyte subset profile compared to knee OA, likely due to the joint's unique anatomical structure and biomechanical function. Zhu et al. employed single-cell RNA sequencing to characterize the cellular and transcriptional landscapes of the condylar cartilage in 3- to 4-month-old human embryos. Their findings revealed distinct cell subsets and gene expression profiles

compared to those observed in the knee joint[30]. Additionally, Zhang et al. explored neurovascular interactions within human condylar cartilage and highlighted the contribution of neurovascular invasion to the progression of TMJOA[31]. In our study, we identified three distinct chondrocyte subsets in the TMJOA condyle: HomCs, preInfCs and InfCs, underscoring the cellular heterogeneity within the condylar cartilage. HomCs exhibit features characteristic of healthy chondrocytes. PreInfCs progressively lose their homeostatic regulatory capacity and transition toward an InfC-like inflammatory phenotype. InfCs, in contrast, display a highly activated inflammatory state and secrete pro-inflammatory mediators.

Cartilage metabolism, including both anabolic and catabolic processes, is essential for maintaining tissue homeostasis and enabling self-repair[32]. As OA progresses, cellular metabolism undergoes profound alterations, including mitochondrial dysfunction and diminished oxidative phosphorylation capacity. These metabolic impairments hinder extracellular matrix synthesis and attenuate anabolic activity. Yang et al. reported that mitochondrial oxidative phosphorylation is suppressed in inflammatory C28/I2 chondrocytes, leading to enhanced fatty acid oxidation and increased reactive oxygen species (ROS) production. This metabolic shift activates the nuclear factor kappa-light-chain-enhancer of activated B cells (NF-κB) signaling pathway, thereby inducing ADAMTS4 overexpression, a key contributor to cartilage degradation in OA[33]. In this study, we found that InfCs exhibit active metabolic processes involving the synthesis of HX and TrX, as well as fatty acid transport, all of which are closely associated with mitochondrial metabolism. These findings suggest that this subset plays a critical role in energy supply. Alterations in fatty acid metabolism and mitochondrial function may promote ROS production and activate downstream inflammatory signaling pathways, thereby contributing to cartilage matrix degradation and the progression of TMJOA.

Further analysis revealed that the InfC subset exhibited marked upregulation of S100a9 and CAMP, with both genes predominantly localized to the pre-hypertrophic and hypertrophic zones of the condylar cartilage in the TMJOA group. S100a9, a member of the S100 calcium-binding protein family, has been widely implicated in osteoarthritis pathogenesis due to its pro-inflammatory and catabolic roles[34]. It activates NF-κB and p38 mitogen-activated protein kinase (p38 MAPK) signaling pathways, thereby promoting the production of inflammatory cytokines such as IL-1β and TNF-α and accelerating cartilage degradation[35,36]. Elevated S100a9 expression has been reported in the synovial tissue, cartilage and peripheral blood of OA patients, supporting its potential as an early diagnostic biomarker[37–39]. CAMP, initially identified as an antimicrobial peptide, has recently been recognized for its dual functions in OA pathophysiology[40]. It suppresses ROS and TNF-α expression through gene methylation, while simultaneously promoting transforming growth factor-β (TGF-β) expression and contributing to chondrocyte apoptosis and matrix remodeling[41]. However, the precise regulatory role of CAMP remains incompletely understood and may vary depending on the inflammatory microenvironment.

Collectively, our findings suggest that S100a9^{+}CAMP^{+} InfCs represent a distinct inflammation-associated chondrocyte subset that emerges under inflammatory stress in TMJOA. Their enrichment in late-stage differentiation zones and strong pro-inflammatory transcriptional profile imply that they may drive terminal chondrocyte differentiation and matrix mineralization, thereby facilitating cartilage

degeneration. These cells may reflect a transitional state from homeostasis to degeneration and represent a TMJOA-specific inflammatory response, providing new insights into disease progression and potential therapeutic targets.

Conclusion

In conclusion, this study identifies three distinct chondrocyte subsets in TMJOA: HomCs, preInfCs and InfCs, highlighting the cellular heterogeneity of condylar chondrocytes in TMJOA. The InfC subset, characterized by co-expression of S100a9 and CAMP, is localized to the prehypertrophic and hypertrophic layers of the condylar cartilage and appears to play a key role in the progression of TMJOA. We hypothesize that the $S100a9^{+}CAMP^{+}$ InfCs subset plays a critical role in the transition of condylar chondrocytes from a healthy to a pathological state under inflammatory conditions. This finding provides a foundation for deeper insights into the pathogenesis of TMJOA and supports the development of precision therapeutic strategies. This study provides novel insights into the pathogenesis of TMJOA, but the specific functional roles of S100a9 and CAMP remain to be fully elucidated. Future studies are needed to investigate the functional role of $S100a9^{+}CAMP^{+}$ InfCs and their regulatory mechanisms in the progression of TMJOA.

Abbreviations

TMJOA	Temporomandibular joint osteoarthritis
MCC	Mandibular condylar cartilage
ScRNA-seq	Single-cell RNA sequencing
HomCs	Homeostatic chondrocytes
preInfCs	Pre-inflammatory chondrocytes
InfCs	Inflammatory chondrocytes
CFA	Complete Freund’s adjuvant
SD	Sprague-Dawley
S100a9	S100 calcium-binding protein a9
CAMP	Cathelicidin antimicrobial peptide
OARSI	Osteoarthritis Research Society International
MMP13	Matrix metalloprotein13
IL-1β	Interleukin-1β
COL2	Collagen Type II
UMAP	Uniform manifold approximation and projection
ADAMTS5	A disintegrin and metalloproteinase with thrombospondin motifs 5
GO	Gene Ontology
KEGG	Kyoto Encyclopedia of Genes and Genomes
DEGs	Differentially expressed genes
TNF-α	Tumor necrosis factor-α

Declarations

Data Availability

The RNA-seq datasets generated and analyzed during the current study are available in the NCBI Sequence Read Archive (SRA) under the BioProject accession number PRJNA1347984 (https://www.ncbi.nlm.nih.gov/bioproject/PRJNA1347984).

Ethical approval and consent to participate

All animal experiments described in this study were approved by the institutional review board (Kunming Medical University Animal Experiments Committee) and conducted according to their guidelines.

Consent for publication

Not applicable.

Availability of data and materials

The datasets used and analyzed during the current study are available from the corresponding author upon reasonable request.

Competing interests

The authors declare that they have no competing interests.

Funding

This work was supported by grants from the Yunnan Revitalization Talent Support Program (XDYC-QNRC-2022-0313), the First-Class Discipline Team of Kunming Medical University (2024XKTDTS08), the Joint Project of Yunnan Provincial Science and Technology Department and Kunming Medical University (202401AY070001-332) and the National Natural Science Foundation of China (82060196 and 82360200).

Authors' contributions

FX, YX, JL and JZ performed all experiments. TX analyzed all bioinformatic data. WW designed the experiments and supervised the research. FX and YX wrote the main manuscript with assistance from JH and WW. All authors reviewed and approved the final manuscript.

Acknowledgments

Not applicable.

References

1. Musumeci G, Castrogiovanni P, Trovato FM, Weinberg AM, Al-Wasiyah MK, Alqahtani MH, et al. Biomarkers of chondrocyte apoptosis and autophagy in osteoarthritis. Int J Mol Sci. 2015;16(9):20560–75.
2. Liu X, Zhao J, Jiang H, Li H, Feng Y, Ke J, et al. ALPK1 Aggravates TMJOA Cartilage Degradation via NF-κB and ERK1/2 Signaling. J Dent Res. SAGE Publications; 2022;101(12):1499–509.
3. Pantoja LLQ, De Toledo IP, Pupo YM, Porporatti AL, De Luca Canto G, Zwir LF, et al. Prevalence of degenerative joint disease of the temporomandibular joint: a systematic review. Clin Oral Investig. Springer Science and Business Media LLC; 2019;23(5):2475–88.
4. Sannajust S, Imbert I, Eaton V, Henderson T, Liaw L, May M, et al. Females have greater susceptibility to develop ongoing pain and central sensitization in a rat model of temporomandibular joint pain.

Pain. 2019;160(9):2036–49.
5. Yang C, Dong W, Wang Y, Dong X, Xu X, Yu X, et al. DDIT3 aggravates TMJOA cartilage degradation via Nrf2/HO-1/NLRP3-mediated autophagy. Osteoarthritis Cartilage. 2024;32(8):921–37.
6. Li B, Guan G, Mei L, Jiao K, Li H. Pathological mechanism of chondrocytes and the surrounding environment during osteoarthritis of temporomandibular joint. J Cell Mol Med. 2021;25(11):4902–11.
7. Roberts WE, Stocum DL. Part II: Temporomandibular Joint (TMJ)-Regeneration, Degeneration, and Adaptation. Curr Osteoporos Rep. 2018;16(4):369–79.
8. Stocum DL, Roberts WE. Part I: development and physiology of the temporomandibular joint. Curr Osteoporos Rep. 2018;16(4):360–8.
9. Xu M, Zhang X, He Y. An Updated View on Temporomandibular Joint Degeneration: Insights from the Cell Subsets of Mandibular Condylar Cartilage. Stem Cells Dev. 2022;31(15–16):445–59.
10. Prein C, Warmbold N, Farkas Z, Schieker M, Aszodi A, Clausen-Schaumann H. Structural and mechanical properties of the proliferative zone of the developing murine growth plate cartilage assessed by atomic force microscopy. Matrix Biol: J Int Soc Matrix Biol. 2016;50:1–15.
11. St-Jacques B, Hammerschmidt M, McMahon AP. Indian hedgehog signaling regulates proliferation and differentiation of chondrocytes and is essential for bone formation. Genes Dev. 1999;13(16):2072–86.
12. Cardoneanu A, Macovei LA, Burlui AM, Mihai IR, Bratoiu I, Rezus II, et al. Temporomandibular joint osteoarthritis: pathogenic mechanisms involving the cartilage and subchondral bone, and potential therapeutic strategies for joint regeneration. Int J Mol Sci. 2022;24(1):171.
13. Qu Y, Wang Y, Wang S, Yu X, He Y, Lu R, et al. A comprehensive analysis of single-cell RNA transcriptome reveals unique SPP1+ chondrocytes in human osteoarthritis. Comput Biol Med. 2023;160:106926.
14. Ammons DT, Chow L, Goodrich L, Bass L, Larson B, Williams ZJ, et al. Characterization of the single cell landscape in normal and osteoarthritic equine joints. Ann Transl Med. 2024;12(5):88.
15. Li X, Liao Z, Deng Z, Chen N, Zhao L. Combining bulk and single-cell RNA-sequencing data to reveal gene expression pattern of chondrocytes in the osteoarthritic knee. Bioengineered. 2021;12(1):997–1007.
16. Gu Y, Hu Y, Zhang H, Wang S, Xu K, Su J. Single-cell RNA sequencing in osteoarthritis. Cell Prolif. 2023;56(12):e13517.
17. Fan Y, Bian X, Meng X, Li L, Fu L, Zhang Y, et al. Unveiling inflammatory and prehypertrophic cell populations as key contributors to knee cartilage degeneration in osteoarthritis using multi-omics data integration. Ann Rheum Dis. 2024;83(7):926–44.
18. Sun H, Wen X, Li H, Wu P, Gu M, Zhao X, et al. Single-cell RNA-seq analysis identifies meniscus progenitors and reveals the progression of meniscus degeneration. Ann Rheum Dis. Elsevier BV; 2020;79(3):408–17.

19. Wang X, Ning Y, Zhang P, Poulet B, Huang R, Gong Y, et al. Comparison of the major cell populations among osteoarthritis, kashin-beck disease and healthy chondrocytes by single-cell RNA-seq analysis. Cell Death Dis. 2021;12(6):551.
20. Glasson SS, Chambers MG, Van Den Berg WB, Little CB. The OARSI histopathology initiative - recommendations for histological assessments of osteoarthritis in the mouse. Osteoarthritis Cartilage. 2010;18 Suppl 3:S17-23.
21. Salo PT, Hogervorst T, Seerattan RA, Rucker D, Bray RC. Selective joint denervation promotes knee osteoarthritis in the aging rat. J Orthop Res. Wiley; 2002;20(6):1256–64.
22. Satija R, Farrell JA, Gennert D, Schier AF, Regev A. Spatial reconstruction of single-cell gene expression data. Nat Biotechnol. 2015;33(5):495–502.
23. Jin S, Guerrero-Juarez CF, Zhang L, Chang I, Ramos R, Kuan C-H, et al. Inference and analysis of cell-cell communication using CellChat. Nat Commun. 2021;12(1):1088.
24. Griss J, Viteri G, Sidiropoulos K, Nguyen V, Fabregat A, Hermjakob H. ReactomeGSA - efficient multi-omics comparative pathway analysis. Mol Cell Proteom: MCP. 2020;19(12):2115–25.
25. Li L, Lv G, Wang B, Kuang L. XIST/miR-376c-5p/OPN axis modulates the influence of proinflammatory M1 macrophages on osteoarthritis chondrocyte apoptosis. J Cell Physiol. 2020;235(1):281–93.
26. Xie J, Huang Z, Yu X, Zhou L, Pei F. Clinical implications of macrophage dysfunction in the development of osteoarthritis of the knee. Cytokine Growth Factor Rev. 2019;46:36–44.
27. Hu X, Li Z, Ji M, Lin Y, Chen Y, Lu J. Identification of cellular heterogeneity and immunogenicity of chondrocytes via single-cell RNA sequencing technique in human osteoarthritis. Front Pharmacol. 2022;13:1004766.
28. Sebastian A, McCool JL, Hum NR, Murugesh DK, Wilson SP, Christiansen BA, et al. Single-cell RNA-seq reveals transcriptomic heterogeneity and post-traumatic osteoarthritis-associated early molecular changes in mouse articular chondrocytes. Cells. 2021;10(6):1462.
29. Ji Q, Zheng Y, Zhang G, Hu Y, Fan X, Hou Y, et al. Single-cell RNA-seq analysis reveals the progression of human osteoarthritis. Ann Rheum Dis. 2019;78(1):100–10.
30. Zhu Q, Tan M, Wang C, Chen Y, Wang C, Zhang J, et al. Single-cell RNA sequencing analysis of the temporomandibular joint condyle in 3 and 4-month-old human embryos. Cell Biosci. 2023;13(1):130.
31. Zhang D, Zhang Y, Xia S, Chen L, Xu W, Huo L, et al. Single-cell RNA sequencing reveals neurovascular-osteochondral network crosstalk during temporomandibular joint osteoarthritis: Pilot study in a human condylar cartilage. Heliyon. 2023;9(10):e20749.
32. Zheng L, Zhang Z, Sheng P, Mobasheri A. The role of metabolism in chondrocyte dysfunction and the progression of osteoarthritis. Ageing Res Rev. 2021;66:101249.
33. Yang K, Xie Q, Liang J, Shen Y, Li Z, Zhao N, et al. Identification of andrographolide as a novel FABP4 inhibitor for osteoarthritis treatment. Phytomed: Int J Phytother Phytopharm. 2023;118:154939.

34. Schelbergen RFP, De Munter W, Van Den Bosch MHJ, Lafeber FPJG, Sloetjes A, Vogl T, et al. Alarmins S100A8/S100A9 aggravate osteophyte formation in experimental osteoarthritis and predict osteophyte progression in early human symptomatic osteoarthritis. Ann Rheum Dis. 2016;75(1):218–25.
35. Kim RY, Sunkara KP, Bracke KR, Jarnicki AG, Donovan C, Hsu AC, et al. A microRNA-21-mediated SATB1/S100A9/NF-κB axis promotes chronic obstructive pulmonary disease pathogenesis. Sci Transl Med. 2021;13(621):eaav7223.
36. Sunahori K, Yamamura M, Yamana J, Takasugi K, Kawashima M, Yamamoto H, et al. The S100A8/A9 heterodimer amplifies proinflammatory cytokine production by macrophages via activation of nuclear factor kappa B and p38 mitogen-activated protein kinase in rheumatoid arthritis. Arthritis Res Ther. 2006;8(3):R69.
37. Ruan G, Xu J, Wang K, Zheng S, Wu J, Ren J, et al. Associations between serum S100A8/S100A9 and knee symptoms, joint structures and cartilage enzymes in patients with knee osteoarthritis. Osteoarthr Cartilage. Elsevier; 2019;27(1):99–105.
38. Geven EJW, van den Bosch MHJ, Di Ceglie I, Ascone G, Abdollahi-Roodsaz S, Sloetjes AW, et al. S100A8/A9, a potent serum and molecular imaging biomarker for synovial inflammation and joint destruction in seronegative experimental arthritis. Arthritis Res Ther. 2016;18(1):247.
39. Schelbergen RF, van Dalen S, ter Huurne M, Roth J, Vogl T, Noël D, et al. Treatment efficacy of adipose-derived stem cells in experimental osteoarthritis is driven by high synovial activation and reflected by S100A8/A9 serum levels. Osteoarthritis Cartilage. 2014;22(8):1158–66.
40. Zhou H, Zou L, Ren H, Shen Z, Lin Y, Cai H, et al. Cathelicidin-BF regulates the AMPK/SIRT1/NF-κB pathway to ameliorate murine osteoarthritis: In vitro and in vivo studie. Int Immunopharmacol. 2024;134:112201.
41. Wang G, Li Y, Yang G, Yang T, He L, Wang Y. Cathelicidin antimicrobial peptide (CAMP) gene promoter methylation induces chondrocyte apoptosis. Hum Genomics. 2021;15(1):24.

Figures

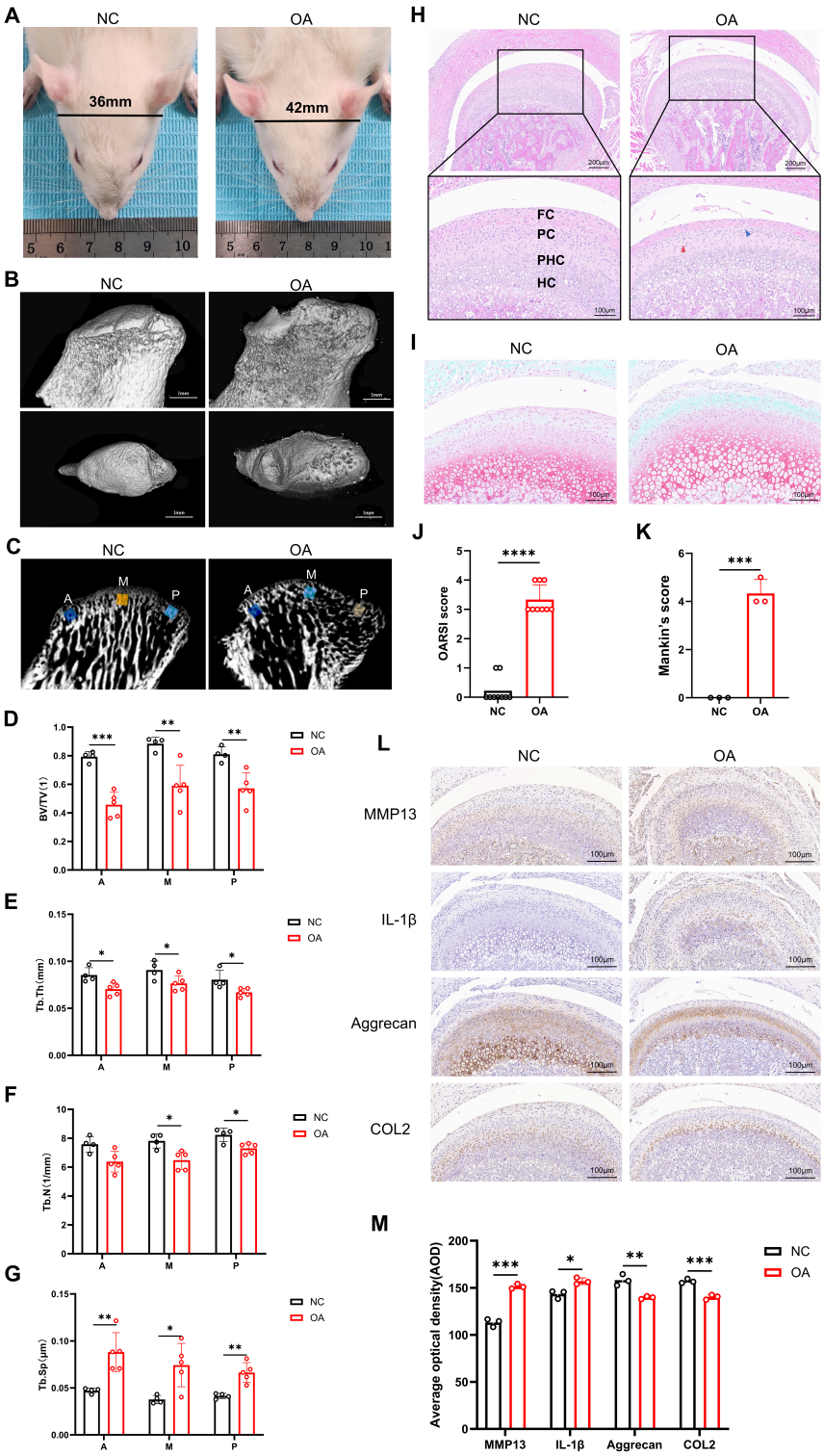


Figure 1

TMJ OA-like defects in CFA intra-articular injection rats. (A) Representative photographs taken ten days after rats received the first saline injection (NC group) or CFA injection (OA group), along with corresponding differences in head widths. Marked swelling was observed in the TMJ region ten days after CFA injection. **(B)** Micro-CT of live images of a sagittal view of the mandibular condyle. Scale bar: 1 mm. **(C)** Schematic illustration of the three selected regions (anterior, middle and posterior, labeled as A,

M, and P in the image) on the sagittal section of the mandibular condyle. **(D**-**G)** Quantification analysis of microarchitecture parameters of the subchondral bone. BV/TV, bone volume/total volume; Tb.Th, Trabecular Thickness; Tb.N, Trabecular Number; Tb.Sp, Trabecular Separation; 1/mm, 1 trabecular number per mm region. **(H)** H&E staining of sagittal TMJ sections. Scale bar: 200 μm (upper), 100 μm (lower). **(I)** Safranin O–Fast Green staining of sagittal TMJ sections. Scale bar: 100 μm. **(J** and **K)** Quantification of Osteoarthritis Research Society International (OARSI) score and modified Mankin score in TMJs. **(L** and **M)** Immunohistochemical results of S100a9, CAMP, IL-1β, MMP13, ADAMTS5 and COL2A1 in the NC and OA groups of rats. Data are represented as mean±SEM calculated by Student's t test. n ≥ 3 rats, *P < 0.05, **P < 0.01, ***P < 0.001, ****P < 0.0001.

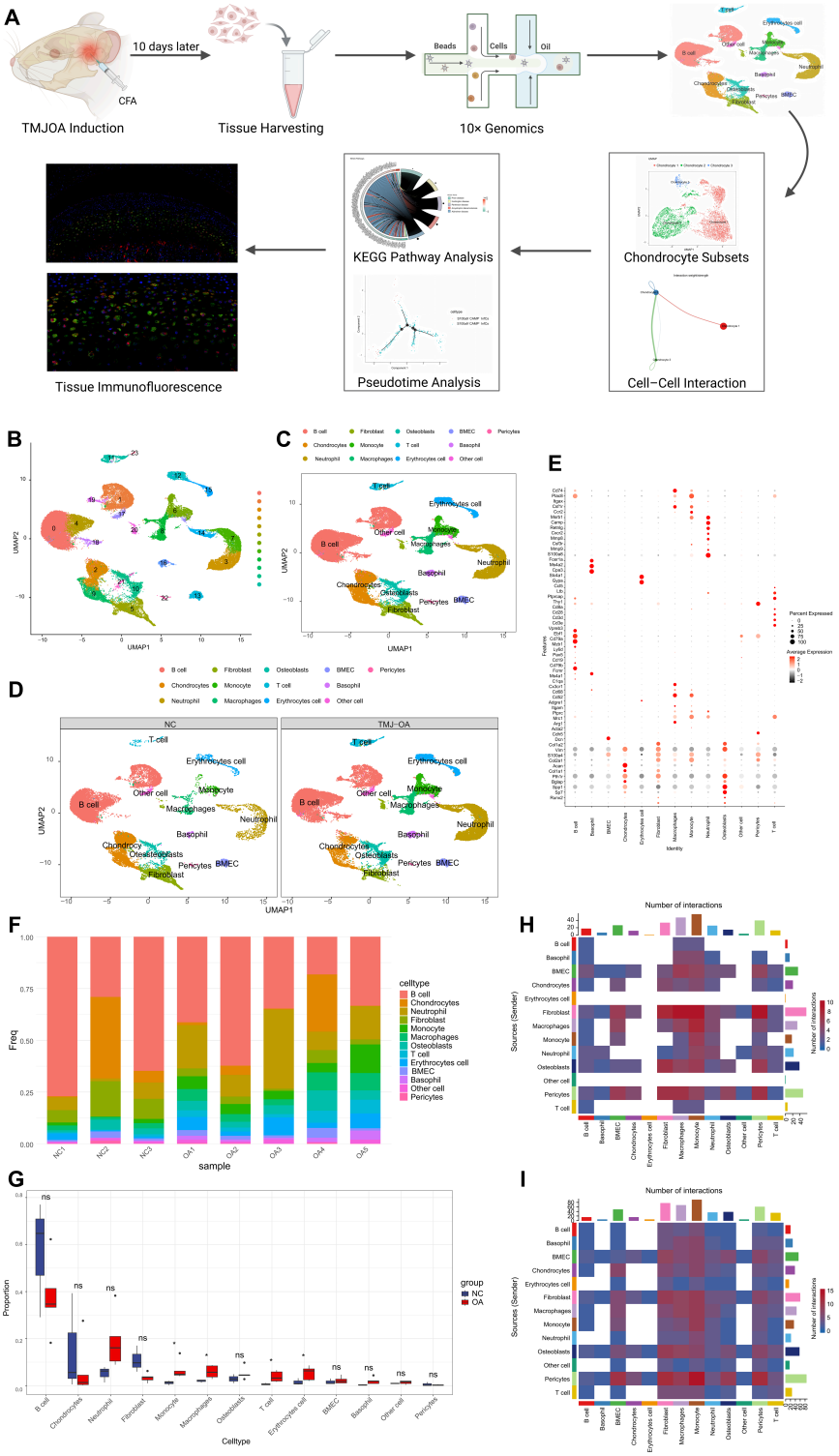


Figure 2

Single-cell landscape of rat condylar tissue. (A) Study flow diagram. **(B)** Initial unsupervised clustering identified distinct cell clusters in rat condylar tissue, n = 53,428 cells. **(C** and **D)** Uniform manifold approximation and projection (UMAP) plot representation of major cell types in rat condylar tissue. **(E)** Bubble plots of the expression levels of marker genes in different cell types. **(F** and **G)** Relative proportional change in total cell numbers between the OA group and the NC group for all clusters shown

in (D). **(H** and **I)** Heatmap of the number of intercellular communications among different cell types in the NC (H) and OA (I) groups.

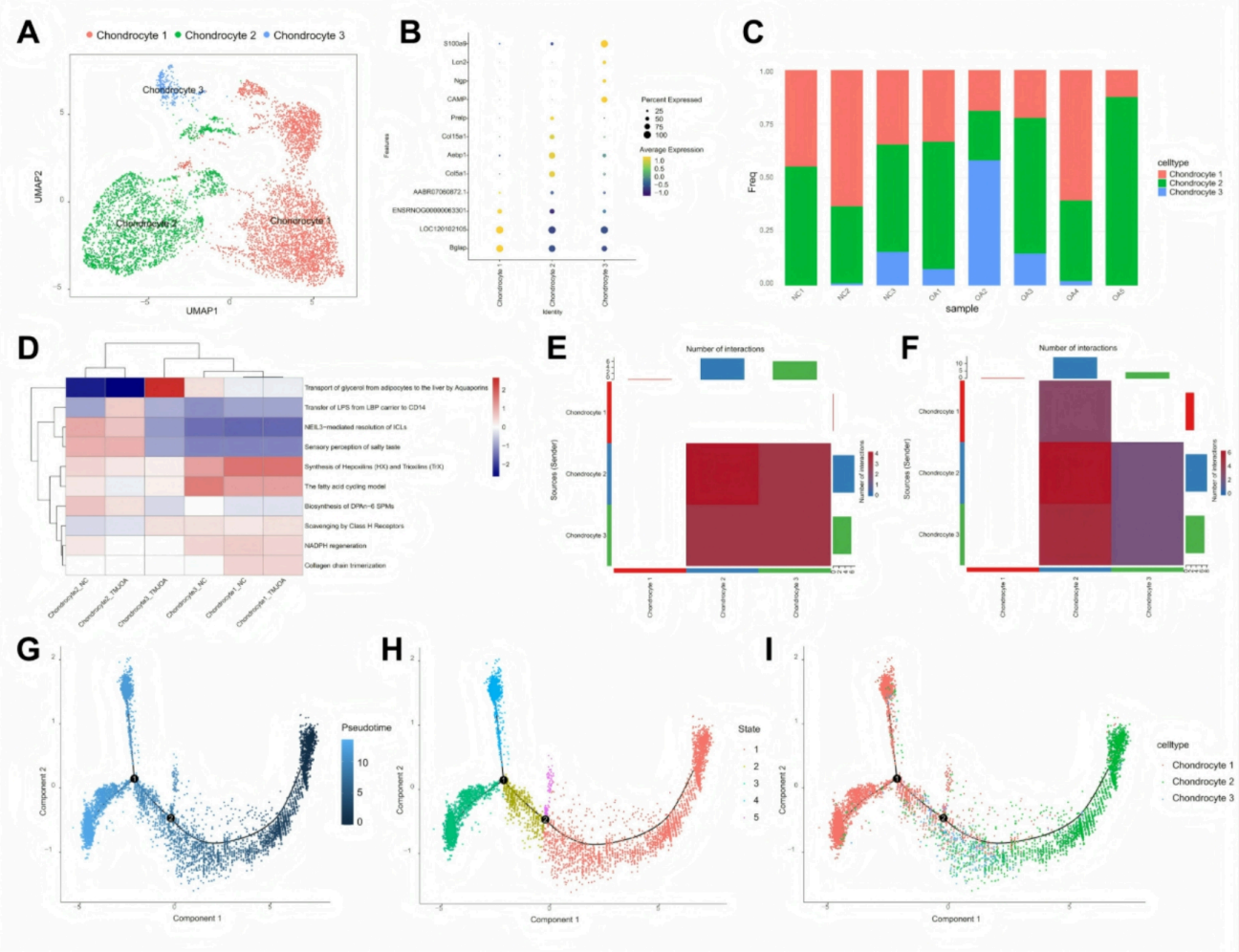


Figure 3

Heterogeneity analysis of chondrocytes. (A) UMAP plot showing the distribution of chondrocyte subsets in rat condylar tissue. **(B)** Bubble plots of the expression levels of marker genes in different chondrocyte subsets. **(C)** Relative proportional change in total cell numbers of all chondrocyte subsets between the OA and NC groups. **(D)** Heatmap showing enriched pathways of different chondrocyte subsets in the NC and OA groups. **(E** and **F)** Heatmap illustrating intercellular communication counts among different chondrocyte subsets in the NC (E) and OA (F) groups. **(G)** Pseudotime trajectory colored in a gradient from dark to light blue, indicating a progression from right to left. The annotated key nodes (1 and 2) may represent critical differentiation stages or state transition points.**(H)** The pseudotime trajectory is shown coloured by different cell states. **(I)** Pseudotime trajectory showing the positions of three chondrocyte subsets during cellular progression.

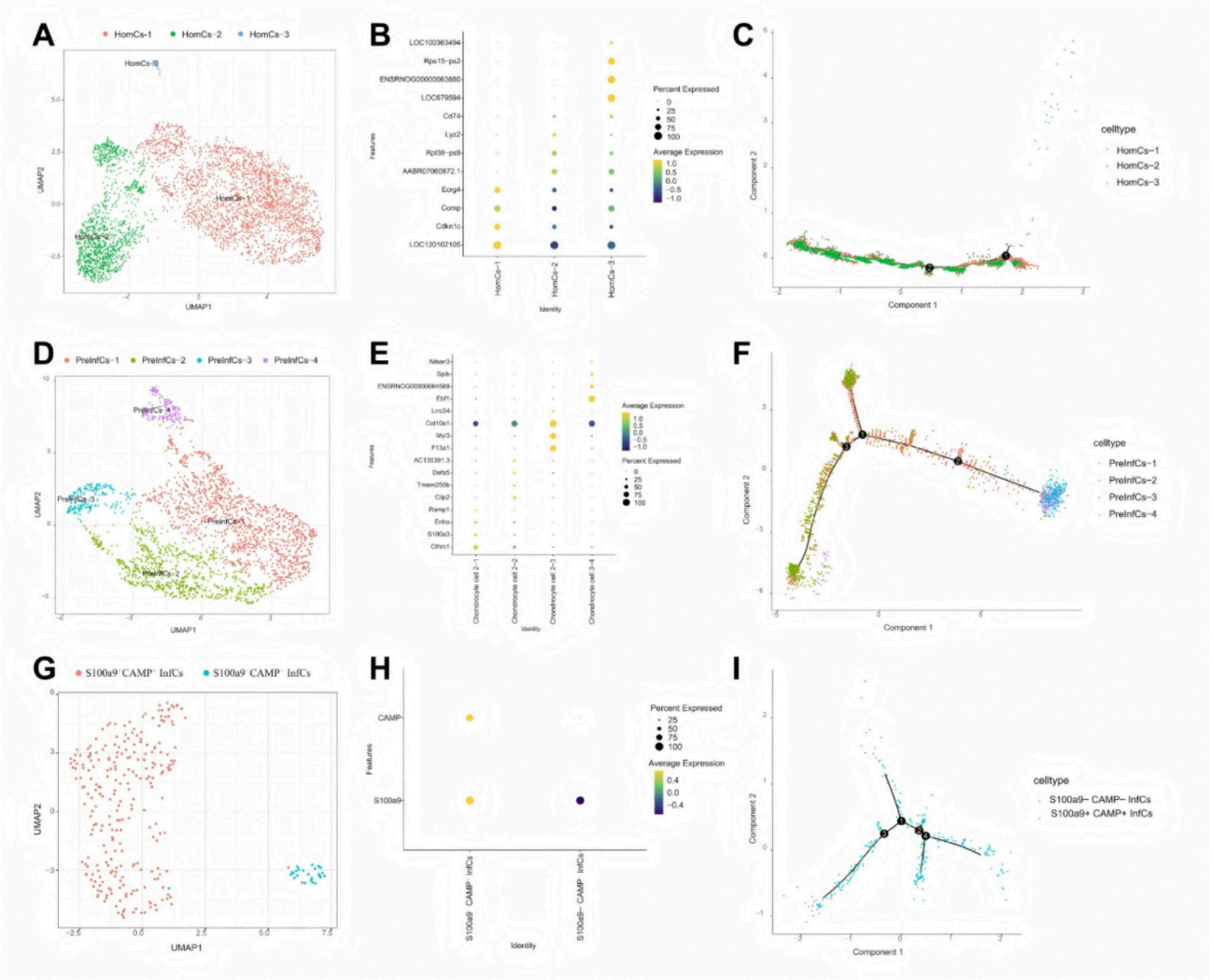


Figure 4

Re-clustering analysis of chondrocyte subsets. (A) The visualisation of the subset of HomCs using UMAP projections, that is, HomCs-1 (red), HomCs-2 (green) and HomCs-3 (blue). **(B)** Bubble plot illustrating the expression of marker genes in individual subsets of HomCs. **(C)** Pseudotime trajectory showing the positions of three HomCs subsets during cellular progression. **(D)** The visualisation of the subset of PreInfCs using UMAP projections, that is, PreInfCs-1 (red), PreInfCs-2 (green), PreInfCs-3 (blue) and PreInfCs-4 (purple). **(E)** Bubble plot illustrating the expression of marker genes in individual subsets of PreInfCs. **(F)** Pseudotime trajectory showing the positions of four PreInfCs subsets during cellular progression. **(G)** The visualisation of the subset of InfCs using UMAP projections, that is, S100a9^{+}CAMP^{+} InfCs (red) and S100a9^{-}CAMP^{-}InfCs (blue). **(H)** Bubble plot illustrating the expression of marker genes in individual subsets of InfCs. **(I)** Pseudotime trajectory showing the positions of two InfCs subsets during cellular progression.

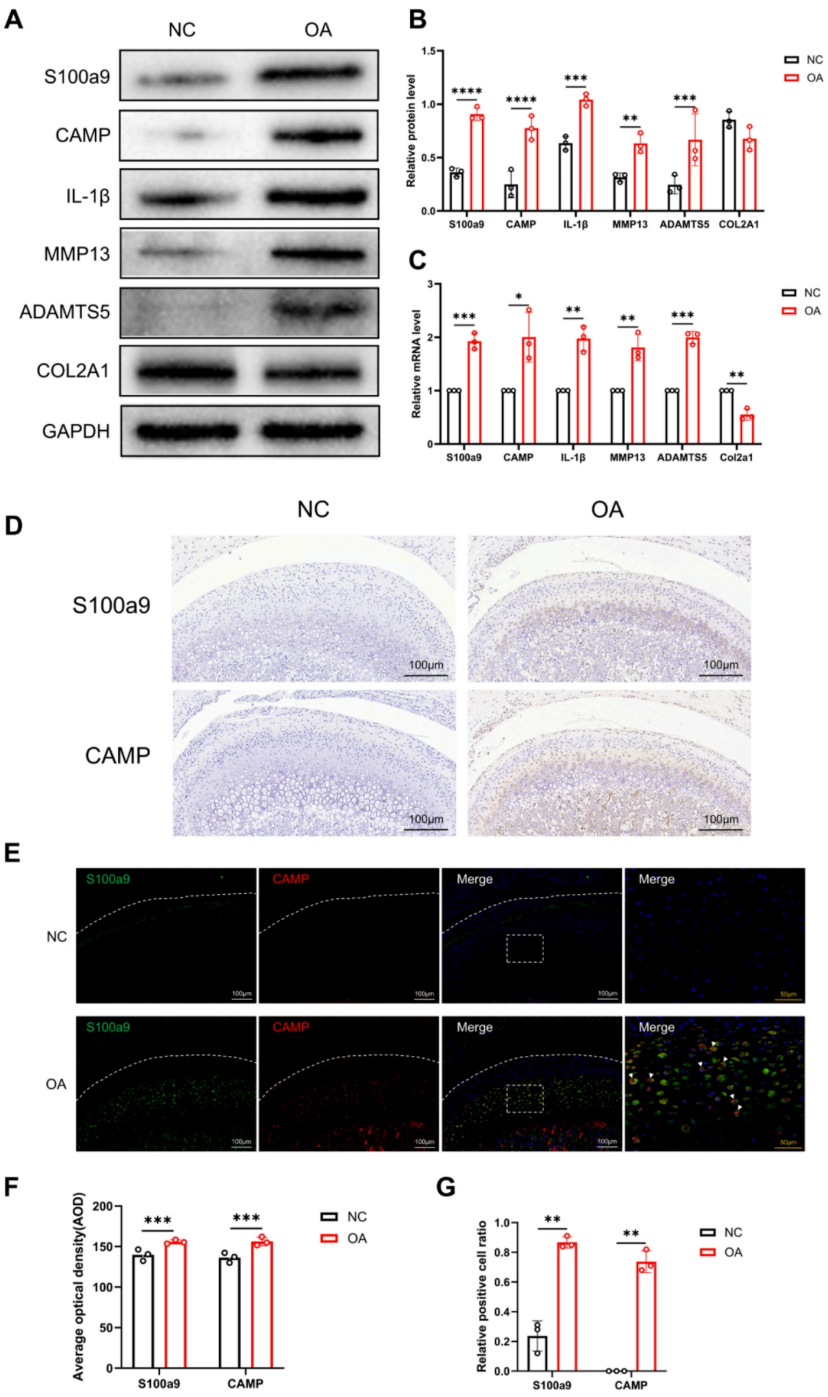


Figure 5

Elevated expression and immunolocalization of disease-associated molecules in TMJ articular cartilage. (A-C) Western blotting results and mRNA levels of S100a9, CAMP, IL-1β, MMP13, ADAMTS5 and COL2A1 in the NC and OA groups of rats. **(D** and **F)** Immunohistochemical results of S100a9 and CAMP in the NC and OA groups of rats. Scale bar: 100 μm. **(E)** Immunofluorescence staining of S100a9 and CAMP in condylar tissues from the NC and OA groups of rats. White scale bar: 100 μm; yellow scale

bar: 50 μm. **(G)** Positive cell rates in fluorescence staining of the NC and OA groups. Data are represented as mean±SEM calculated by Student's t test. n ≥ 3 rats, *P < 0.05, **P < 0.01, ***P < 0.001, ****P < 0.0001.

Supplementary Files

This is a list of supplementary files associated with this preprint. Click to download.

- UncroppedWesternBlots.docx
- Supplementaryfigures.docx